

# SCALABLE OPTIMIZATION-BASED SAMPLING ON FUNCTION SPACE

ZHENG WANG\*, TIANGANG CUI†, JOHNATHAN M. BARDSLEY‡, AND YOUSSEF M. MARZOUK\*

**Abstract.** Optimization-based samplers provide an efficient and parallelizable approach to solving large-scale Bayesian inverse problems. These methods solve randomly perturbed optimization problems to draw samples from an approximate posterior distribution. “Correcting” these samples, either by Metropolization or importance sampling, enables characterization of the original posterior distribution. This paper presents a new geometric interpretation of the randomize-then-optimize (RTO) method [1] and a unified transport-map interpretation of RTO and other optimization-based samplers, i.e., implicit sampling [19] and randomized-maximum-likelihood [20]. We then introduce a new subspace acceleration strategy that makes the computational complexity of RTO scale linearly with the parameter dimension. This subspace perspective suggests a natural extension of RTO to a function space setting. We thus formalize a function-space version of RTO and establish sufficient conditions for it to produce a valid Metropolis–Hastings proposal, yielding *dimension-independent* sampling performance. Numerical examples corroborate the dimension-independence of RTO and demonstrate sampling performance that is also robust to small observational noise.

**Key words.** Markov chain Monte Carlo, Metropolis independence sampling, Bayesian inference, infinite-dimensional inverse problems

**AMS subject classifications.** 15A29, 65C05, 65C60

**1. Introduction.** The Bayesian statistical approach is widely used for uncertainty quantification in inverse problems—i.e., inferring parameters of mathematical models given indirect, limited, and/or noisy data [15, 27]. In a Bayesian setting, the parameters are described as random variables and endowed with prior distributions. Conditioning on a realized value of the data yields the posterior distribution of these parameters, which characterizes uncertainty in possible parameter values. Solving the inverse problem amounts to computing posterior expectations, e.g., posterior means, variances, marginals, or other quantities of interest.

Sampling methods—in particular, Markov chain Monte Carlo (MCMC) algorithms—provide an extremely flexible way of estimating posterior expectations [4]. The design of effective MCMC methods, however, rests on the careful construction of proposal distributions: efficiency demands proposal distributions that reflect the geometry of the posterior [12], e.g., anisotropy, strong correlations, and even non-Gaussianity [21]. Another significant challenge in applying MCMC is parameter dimensionality. In many inverse problems governed by partial differential equations, the “parameter” is in fact a function of space and/or time that, for computational purposes, must be represented in a discretized form. Discretizations that sufficiently resolve the spatial or temporal heterogeneity of this function are often high dimensional. Yet, as analyzed in [17, 18, 24, 25], the performance of many common MCMC algorithms may degrade as the dimension of the discretized parameter increases, meaning that more MCMC iterations are required to obtain an effectively independent sample. One can design MCMC algorithms that do not degrade in this manner by formulating them in function space and ensuring that the proposal distribution satisfies a certain absolute continuity condition [8, 27]. These samplers are called *dimension independent* [8, 9]. Yet another core challenge is that MCMC algorithms are, in general, intrinsically serial: sampling amounts to simulating a discrete-time Markov process. The literature has seen many attempts at parallelizing the evaluation of proposed points [5] or sharing information across multiple chains [7, 14], but none of these is embarrassingly parallel.

A promising approach to many of these challenges is to *convert optimization methods into samplers* (i.e., Monte Carlo methods). This idea has been proposed in many forms: key examples

\*Center for Computational Engineering, Massachusetts Institute of Technology, Cambridge, MA 02139 USA (zheng\_w@mit.edu, ymarz@mit.edu)

†School of Mathematical Sciences, Monash University, Victoria 3800, Australia (tiangang.cui@monash.edu)

‡Department of Mathematical Sciences, Montana, University of Montana, Missoula, MT 59812 USA (bardsleyj@mso.umt.edu)

include randomize-then-optimize (RTO) [1], Metropolized randomized-maximum-likelihood (RML) [20, 28], and implicit sampling [6, 19]. In its most basic form, RTO requires Bayesian inverse problems with Gaussian priors and noise models, although it can extend to problems with non-Gaussian priors via a change of variables [29]. Metropolized RML has problem requirements similar to those of RTO, but requires evaluating second-order derivatives of the forward model. Implicit sampling applies to target densities whose contours enclose star-convex regions, in that any ray starting from the mode (or some other nominal point) intersects each contour only once; each proposal sample can then be generated cheaply by solving a line search.

In general, each of these algorithms solves randomly-perturbed realizations of an optimization problem to generate samples from a probability distribution that is “close to” the posterior. The probability density function of this distribution is computable, and thus the distribution can be used as an independent proposal within MCMC or as a biasing distribution in importance sampling. For non-Gaussian targets, these proposal distributions are non-Gaussian. In general, they are *adapted* to the target distribution. The computational complexity and dimension-scalability of the resulting sampler can be linked to the structure of the corresponding optimization problem. In addition, these sampling methods are embarrassingly parallel, and are easily implemented with existing optimization tools developed for solving deterministic inverse problems.

This paper considers optimization-based sampling in high dimensions. We focus on the analysis and scalable implementation of the RTO method. To begin, we present a new geometric interpretation of RTO that provides intuition for the method and its regime of applicability (Section 2). We also interpret RTO and other optimization-based samplers as ways of realizing the actions of particular *transport maps* [16] (Section 3). Using these two interpretations, we next motivate and construct a subspace-accelerated version of RTO whose computational complexity scales linearly with parameter dimension (Section 4). This approach significantly accelerates RTO in high-dimensional settings. Subspace acceleration reveals that RTO’s mapping acts differently on different subspaces of the parameter space. Exploiting the separation of the parameter subspaces allows us to cast the transport map generated by RTO in an infinite-dimensional (i.e., function space) setting [27] (Section 5). As our main theoretical result, we establish sufficient conditions for the probability distribution induced by RTO’s mapping to be absolutely continuous with respect to the posterior. This result justifies RTO’s observed *dimension-independent* sampling behavior: the acceptance rate and autocorrelation time of an MCMC chain using RTO as its proposal do not degrade as the parameter dimension increases. Similarly, the performance of importance sampling using RTO as a biasing distribution will stabilize in high dimensions. This result is analogous to the arguments in [3, 27, 9, 2, 26] showing that (generalized) preconditioned Crank–Nicolson (pCN), dimension-independent likelihood-informed (DILI) MCMC, and other infinite-dimensional geometric MCMC methods are dimension-independent. However, our MCMC construction relies on non-Gaussian proposals in a Metropolis independence setting, where the Markov chain can be run at essentially zero cost *after* the computationally costly step of drawing proposal samples and evaluating the proposal density. Because the latter step is embarrassingly parallel, the overall MCMC scheme is immediately parallelizable, unlike the above-mentioned MCMC samplers that rely on the iterative construction of Markov chains.

In Section 6, we provide a numerical illustration of our algorithms, exploring the factors that influence RTO’s sampling efficiency. We observe that neither the parameter dimension nor the magnitude of the observational noise influence RTO’s performance *per MCMC step*, though they both impact the computational cost of each step. Despite its more costly steps, RTO outperforms simple pCN in this example. Overall, our results show that RTO can tackle inverse problems with large parameter dimensions and arbitrarily small observational noise.

**2. RTO and its geometric interpretation.** RTO generates samples from an approximation to the target distribution in two steps. First, it repeatedly solves perturbed optimization problems to generate independent proposal samples. Second, it uses this collection of samples to describe an

independent proposal within Metropolis–Hastings (MH) or a biasing distribution in self-normalized importance sampling. In this section, we will describe the target distributions to which RTO can be applied and detail the two steps above. We will also present a geometric interpretation in which the RTO proposal can be viewed as a projection. This interpretation helps understand the sampling efficiency of RTO and the technical requirements for the RTO procedure to be valid.

**2.1. Target distribution.** As formulated in [1], RTO applies to target distributions on  $\mathbb{R}^n$  whose densities can be written as

$$(1) \quad \pi_{\text{tar}}(v) \propto \exp\left(-\frac{1}{2} \|H(v)\|^2\right),$$

where  $H : \mathbb{R}^n \rightarrow \mathbb{R}^{m+n}$  is a vector-valued function of the parameters  $v \in \mathbb{R}^n$  with an output dimension of  $n + m$ , for any  $m \geq 1$ . This structure is found in Bayesian inverse problems and other similar problems with  $n$  parameters,  $m$  observations, a Gaussian prior, and additive Gaussian observational noise. To illustrate, let

$$y = F(u) + \epsilon, \quad \epsilon \sim \text{N}(0, \Gamma_{\text{obs}}), \quad u \sim \text{N}(m_{\text{pr}}, \Gamma_{\text{pr}}),$$

where  $y \in \mathbb{R}^m$  is the data,  $F : \mathbb{R}^n \rightarrow \mathbb{R}^m$  is the forward model,  $u \in \mathbb{R}^n$  is the unknown parameter, and  $\epsilon \in \mathbb{R}^m$  is the additive noise, assumed independent of  $u$ . Here,  $m_{\text{pr}}$  is the prior mean, and  $\Gamma_{\text{obs}}$  and  $\Gamma_{\text{pr}}$  are the covariance matrices of the observational noise and prior. We can simplify the problem via an affine change of variables that transforms the covariance matrices to identity matrices. Let us define the matrix square roots,

$$S_{\text{pr}} S_{\text{pr}}^\top := \Gamma_{\text{pr}}, \quad S_{\text{obs}} S_{\text{obs}}^\top := \Gamma_{\text{obs}},$$

and new whitened variables,

$$v := S_{\text{pr}}^{-1}(u - m_{\text{pr}}), \quad G(v) := S_{\text{obs}}^{-1} [F(S_{\text{pr}} v + m_{\text{pr}}) - y], \quad e := S_{\text{obs}}^{-1} \epsilon,$$

where  $v \in \mathbb{R}^n$  is the whitened unknown parameter,  $G : \mathbb{R}^n \rightarrow \mathbb{R}^m$  is the whitened forward model, and  $e$  is the whitened observational noise. The inverse problem becomes

$$0 = G(v) + e, \quad e \sim \text{N}(0, \text{I}), \quad v \sim \text{N}(0, \text{I}).$$

The data is shifted to the origin after whitening. The posterior density of the whitened variable  $v$  is then

$$p(v|y) = \pi_{\text{tar}}(v) \propto \exp\left(-\frac{1}{2} \left\| \begin{bmatrix} v \\ G(v) \end{bmatrix} \right\|^2\right),$$

which is in the required form (1) with  $H$  defined as

$$(2) \quad H(v) := \begin{bmatrix} v \\ G(v) \end{bmatrix}.$$

Given a sample  $v$  from the target density  $\pi_{\text{tar}}(v)$ , we can obtain a posterior sample of the original parameter  $u$  by applying the transformation

$$u = S_{\text{pr}} v + m_{\text{pr}}.$$

Notice that the form of  $\pi_{\text{tar}}(v)$  in (1) is identical to the probability density function of an  $(n + m)$ -dimensional standard normal distribution,  $\pi(w) \propto \exp(-\frac{1}{2} \|w\|^2)$ , evaluated at  $w = H(v)$ . This paints the following geometric picture of the required target distribution: the target density  $\pi_{\text{tar}}(v)$ , up to a normalizing constant, is the same as the density of the  $(n + m)$ -dimensional Gaussian distribution evaluated on the  $n$ -dimensional manifold  $H(v) = (v, G(v)) \subset \mathbb{R}^{m+n}$  parameterized by  $v \in \mathbb{R}^n$ .

**2.2. The RTO algorithm.** The RTO algorithm requires an orthonormal basis for an  $n$ -dimensional subspace of  $\mathbb{R}^{n+m}$ . Let this basis be collected in a matrix  $Q$ ; in principle,  $Q$  can be any  $(n+m) \times n$  matrix with orthonormal columns. One common choice of  $Q$  follows from first finding a linearization point, which is often (but not necessarily) taken to be the mode of the target distribution, i.e.,

$$(3) \quad v_{\text{MAP}} = \arg \min_v \frac{1}{2} \|H(v)\|^2.$$

Then one can compute  $Q$  from a thin QR factorization of  $\nabla H(v_{\text{MAP}})$ ; this sets the basis to span the range of  $\nabla H(v_{\text{MAP}})$ .

Using this matrix, we obtain proposal samples  $v_{\text{prop}}^{(i)}$  by repeatedly drawing independent  $(n+m)$ -dimensional standard normal vectors  $\eta^{(i)}$  and solving the nonlinear system of equations

$$(4) \quad Q^\top H(v_{\text{prop}}^{(i)}) = Q^\top \eta^{(i)},$$

which is equivalent to solving the optimization problem

$$(5) \quad v_{\text{prop}}^{(i)} = \arg \min_v \frac{1}{2} \|Q^\top (H(v) - \eta^{(i)})\|^2,$$

if the minimum of (5) is zero. To ensure that the system of equations (4) has a unique solution and that the probability density of the resulting samples can be calculated explicitly, we require additional conditions as follows.

ASSUMPTION 1 (Sufficient conditions for valid RTO [1]).

1. The function  $H$  is continuously differentiable with Jacobian  $\nabla H$ .
2. The Jacobian  $\nabla H(v)$  has full column rank for every  $v$ .
3. The map  $v \mapsto Q^\top H(v)$  is invertible.

Under these conditions, the RTO samples are distributed according to the probability density

$$(6) \quad q(v) = \pi_{\text{RTO}}(v) \propto |\det(Q^\top \nabla H(v))| \exp\left(-\frac{1}{2} \|Q^\top H(v)\|^2\right).$$

Most of these assumptions follow from the inverse problem setup; for example, it is natural for the forward model to be continuous and the prior to be a proper distribution. The final assumption, however, is more delicate and may not always hold. We will use the geometric interpretation of RTO to elaborate on this assumption.

Proposal samples generated via RTO can be interpreted as a projection of  $(n+m)$ -dimensional Gaussian samples onto the  $n$ -dimensional manifold  $\{H(v) : v \in \mathbb{R}^n\}$ . The samples are projected along the directions orthogonal to the range of  $Q$ . Figure 1 depicts the steps of RTO's proposal for the case  $n = m = 1$ . This geometric interpretation also illustrates conditions for the RTO procedure to be valid: there should exist only one point that is both on the manifold and along the projection directions of  $\eta$ . Under these conditions, the nonlinear system of equations (4) has a unique solution. If a projection of  $\eta^{(i)}$  in the  $Q^\top$  direction onto  $H(v)$  does not exist, or if there exists more than one intersection point, then the RTO procedure breaks down.

As shown in [1], RTO's proposal is exact (i.e., is the target) when the forward model is linear, and its proposal is expected to be close to the target when the forward model is close to linear. For weakly nonlinear problems, the proposal can be a good approximation to the posterior and hence can be used in MCMC and importance sampling.

These proposal samples are used either as an independent proposal in Metropolis–Hastings (MH) or as a biasing distribution in self-normalized importance sampling. For the former case, the Metropolis–Hastings acceptance ratio can be written as

$$\frac{\pi_{\text{tar}}(v_{\text{prop}}^{(i)}) q(v^{(i-1)})}{\pi_{\text{tar}}(v^{(i-1)}) q(v_{\text{prop}}^{(i)})} = \frac{w(v_{\text{prop}}^{(i)})}{w(v^{(i-1)})},$$

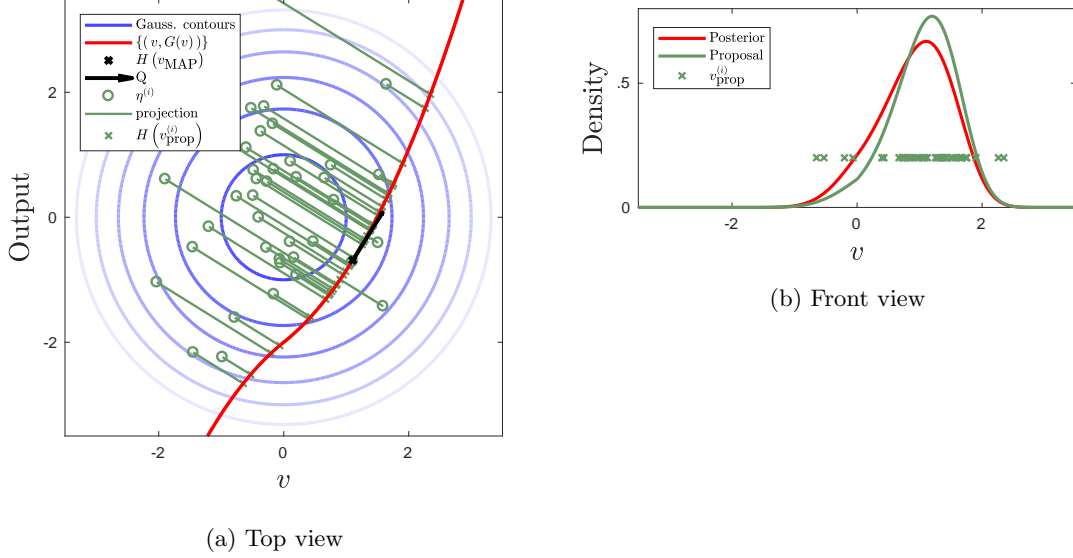


Fig. 1: Interpretation of RTO as a projection, in the case  $n = m = 1$ . The  $(n + m)$ -dimensional Gaussian samples  $\eta$  (green circles), are projected onto the manifold  $\{H(v)\}$  (red line), to determine the proposal samples  $v_{\text{prop}}$  (green x's). The projection is orthogonal to the range of  $Q$ . In the front view, the proposal samples  $v_{\text{prop}}$  (green x's) are shown to be distributed according to a proposal density (green line) that is close to the target density (red line).

where the weight  $w(v)$  is defined as

$$(7) \quad w(v) = |\det(Q^\top \nabla H(v))|^{-1} \exp\left(-\frac{1}{2} \|H(v)\|^2 + \frac{1}{2} \|Q^\top H(v)\|^2\right).$$

The resulting method, called RTO-MH, is summarized in Algorithm 1.

For importance sampling, since the normalizing constant of the target density is unknown, the weights must be normalized as

$$\tilde{w}(v^{(i)}) = w(v^{(i)}) / \sum_{j=1}^N w(v^{(j)}),$$

where  $N$  is the number of samples and the sum of weights  $\tilde{w}(v^{(i)})$  is thus one. The proposal samples and weights can then be used to compute posterior expectations of some quantity of interest  $g(v)$  using the self-normalizing importance sampling formula:

$$\int g(v) \pi_{\text{tar}}(v) dv = \sum_{i=1}^N \tilde{w}(v_{\text{prop}}^{(i)}) g(v_{\text{prop}}^{(i)}).$$

**3. Optimization-based samplers as transport maps.** One can also interpret RTO as a means of *pushing forward* a Gaussian reference distribution to some approximation of the target distribution. In other words, RTO realizes the action of a particular transport map [21]. This interpretation also extends to other optimization-based samplers.

---

**Algorithm 1** RTO Metropolis–Hastings (RTO-MH)

---

```

1: Find  $v_{\text{MAP}}$  using (3)
2: Determine  $\nabla H(v_{\text{MAP}})$ 
3: Compute  $Q$ , whose columns are an orthonormal basis for the range of  $\nabla H(v_{\text{MAP}})$ 
4: for  $i = 1, \dots, n_{\text{samps}}$  do in parallel
5:   Sample  $\eta^{(i)}$  from an  $(n + m)$ –dimensional standard normal distribution
6:   Solve for a proposal sample  $v_{\text{prop}}^{(i)}$  using (5)
7:   Compute  $w(v_{\text{prop}}^{(i)})$  from (7)
8: Set  $v^{(0)} = v_{\text{MAP}}$ 
9: for  $i = 1, \dots, n_{\text{samps}}$  do in series
10:   Sample  $t$  from a uniform distribution on  $[0, 1]$ 
11:   if  $t < w(v_{\text{prop}}^{(i)}) / w(v^{(i-1)})$  then
12:      $v^{(i)} = v_{\text{prop}}^{(i)}$ 
13:   else
14:      $v^{(i)} = v^{(i-1)}$ 

```

---

Recall that RTO solves the following nonlinear system of equations

$$Q^\top H(v) = Q^\top \eta, \quad \text{where } \eta \sim \mathcal{N}(0, \mathbf{I}_{n+m}).$$

Since  $\eta \in \mathbb{R}^{n+m}$  is a standard Gaussian and the columns of  $Q$  are orthonormal, the projection of  $\eta$ , denoted by  $\xi := Q^\top \eta \in \mathbb{R}^n$ , is also a standard Gaussian. This way, the nonlinear system of equations can be expressed as

$$(8) \quad Q^\top H(v) = \xi, \quad \text{where } \xi \sim \mathcal{N}(0, \mathbf{I}_n).$$

This equation describes a deterministic coupling between the target random variable  $v \in \mathbb{R}^n$  and the standard Gaussian “reference” random variable  $\xi \in \mathbb{R}^n$ . The coupling is defined by the forward model, the data, the observational noise, and the prior, through the function  $H$  and the matrix  $Q$ .

The left hand side of (8), which we write compactly as

$$S(\cdot) = Q^\top H(\cdot),$$

defines a transport map from  $v$  to  $\xi$ . By solving the nonlinear system (8) for a given  $\xi$  to obtain a proposal  $v$ , the RTO procedure implicitly inverts the transport map  $S$ ; that is, it evaluates  $S^{-1}$  on each  $\xi$ ,  $v = S^{-1}(\xi)$ . The inverse map  $T = S^{-1}$  pushes forward the reference distribution  $\pi_{\text{ref}} = \mathcal{N}(0, \mathbf{I}_n)$  to an approximation of  $\pi_{\text{tar}}$ . In particular, the normalized probability density of  $v$  generated by RTO is given by the standard formula for pushforward densities:

$$\begin{aligned}
\pi_{\text{RTO}}(v) &= ((S^{-1})_\# \pi_{\text{ref}})(v) \\
&= |\det \nabla S(v)| \pi_{\text{ref}}(S(v)) \\
&= |\det (Q^\top \nabla H(v))| (2\pi)^{-\frac{n}{2}} \exp\left(-\frac{1}{2} \|Q^\top H(v)\|^2\right).
\end{aligned}$$

This transport map interpretation explains why Assumption 1.3 in the previous section is necessary for the validity of the RTO procedure. The transport map interpretation and the geometric interpretation both describe taking a Gaussian random variable  $\xi$  and transforming it through a projection to obtain the proposal random variable  $v$ .

Other optimization-based sampling algorithms such as the random-map implementation of implicit sampling [19] and Metropolized RML [20] similarly yield deterministic couplings of two random

variables. A summary of each algorithm’s mapping is given in Table 1. Each algorithm describes a different map  $S$  and uses computation (i.e., solves an optimization problem) to evaluate  $S^{-1}$ . Detailed derivations of these mappings are provided in Appendix A.

Table 1: Transport map interpretation of the three optimization-based samplers. In RTO, with default settings, the matrix  $Q$  comes from a thin QR factorization, and in implicit sampling, the matrix  $L$  comes from any matrix square root.

Algorithm	Target distribution $\pi_{\text{tar}}(v)$	Transport map $S(v) = \xi$
RTO	$\exp(-\frac{1}{2}\ H(v)\ ^2)$	$Q^\top H(v) = \xi$ where $QR := \nabla H(v_{\text{MAP}})$
Implicit sampling	$\exp(-\Phi(v))$	$\begin{cases} \frac{L^{-1}(v - v_{\text{MAP}})}{\ L^{-1}(v - v_{\text{MAP}})\ } = \frac{\xi}{\ \xi\ } \\ \Phi(v) - \Phi(v_{\text{MAP}}) = \frac{1}{2}\ \xi\ ^2 \end{cases}$ where $L^\top L := [\nabla^2 \Phi(v_{\text{MAP}})]^{-1}$
Metropolized RML	$\exp(-\frac{1}{2}\ v_x\ ^2 - \frac{1}{2}\ g(v_x)\ ^2 - \frac{1}{2\gamma(1-\gamma)}\ v_d - g(v_x) + \gamma g(v_x)\ ^2)$	$\begin{cases} v_x + \frac{1}{\rho}\nabla g(v_x)^\top (g(v_x) - v_d) = \xi_x \\ \frac{1}{\rho}v_d - \left(\frac{1-\rho}{\rho}\right)g(v_x) = \xi_d \end{cases}$ where $\rho$ close to 1, $\gamma$ close to 0

All three algorithms use a standard normal as the reference distribution and the pushforward of this reference through  $S^{-1}$  as a proposal distribution. The proposal distribution is then used as an independent proposal in Metropolis–Hastings or as a biasing distribution in importance sampling. By specifying different relationships between  $\xi$  and  $v$ —that is, different choices of the mapping  $S(v) = \xi$ —we can derive all of these optimization-based samplers in a unified framework.

**4. Scalable implementation of RTO.** Solving the optimization problem (5) and computing the RTO probability density (6) can be computationally costly when the parameter vector  $v$  is high-dimensional. For example, the matrix–vector product with  $Q^\top$  in each evaluation of (5) costs  $O((n+m) \times n)$  floating point operations, and computing the determinant in the proposal density (6) scales as  $O(n^3)$ , where  $n$  is the number of parameters. In this section, we introduce a subspace acceleration strategy to make these operations of RTO scale linearly with the parameter dimension.

This scalable implementation avoids computing and storing the QR factorization of the full-rank  $(n+m) \times n$  matrix  $\nabla H(v_{\text{MAP}})$ . Instead, it opts to construct (and store) a singular value decomposition (SVD) of the smaller  $m \times n$  linearized forward model  $\nabla G(v_{\text{MAP}})$ . This way, the computational complexity of the evaluation of the determinant in (6) and the matrix–vector product with  $Q^\top$  in (5) can scale linearly with the parameter dimension  $n$ .

To begin, we note from the definition (2) of  $H$  that

$$\nabla H(v) = \begin{bmatrix} \mathbf{I} \\ \nabla G(v) \end{bmatrix}.$$

Recall from RTO’s mapping (8) that the RTO proposal samples are found by

$$Q^\top H(v) = \xi, \quad \text{where } \xi \sim \mathcal{N}(0, \mathbf{I}_n),$$

where the columns of  $Q$  form an orthonormal basis for the range of  $\nabla H(v_{\text{MAP}})$  and  $Q$  is computed from the thin QR decomposition of  $\nabla H(v_{\text{MAP}})$ . To avoid computing with the dense  $(m+n) \times n$



matrix  $Q$ , we use instead

$$\tilde{Q} := \nabla H(v_{\text{MAP}}) (\nabla H(v_{\text{MAP}})^\top \nabla H(v_{\text{MAP}}))^{-1/2},$$

which can be shown to have orthonormal columns and the same range as  $\nabla H(v_{\text{MAP}})$ . If the SVD of  $\nabla G(v_{\text{MAP}})$ , which we assume has rank  $r$ , is given by  $\nabla G(v_{\text{MAP}}) =: \Psi \Lambda \Phi^\top$ , then

$$(\nabla H(v_{\text{MAP}})^\top \nabla H(v_{\text{MAP}}))^{-1/2} = \Phi(\Lambda^2 + \mathbf{I}_r)^{-1/2} \Phi^\top + (\mathbf{I}_n - \Phi \Phi^\top),$$

where  $\mathbf{I}_r$  and  $\mathbf{I}_n$  are the identity matrices of size  $r \times r$  and  $n \times n$ , respectively. Using the last identity, we obtain, after some algebraic manipulation,

$$\tilde{Q} = \begin{bmatrix} \Phi(\Lambda^2 + \mathbf{I}_r)^{-1/2} \Phi^\top + (\mathbf{I}_n - \Phi \Phi^\top) \\ \Psi \Lambda (\Lambda^2 + \mathbf{I}_r)^{-1/2} \Phi^\top \end{bmatrix}.$$

which we use to obtain

$$\begin{aligned} \tilde{Q}^\top H(v) &= \left[ \Phi(\Lambda^2 + \mathbf{I}_r)^{-1/2} \Phi^\top + (\mathbf{I}_n - \Phi \Phi^\top) \right] v + \Phi \Lambda (\Lambda^2 + \mathbf{I}_r)^{-1/2} \Psi^\top G(v) \\ (9) \quad &= \Phi \left[ (\Lambda^2 + \mathbf{I}_r)^{-1/2} \Phi^\top v + \Lambda (\Lambda^2 + \mathbf{I}_r)^{-1/2} \Psi^\top G(v) \right] + (\mathbf{I}_n - \Phi \Phi^\top) v. \end{aligned}$$

Thus the nonlinear system  $\tilde{Q}^\top H(v) = \xi$  solved in Step 6 of Algorithm 1 can be rewritten as

$$(10) \quad \begin{cases} (\mathbf{I}_n - \Phi \Phi^\top) \xi = (\mathbf{I}_n - \Phi \Phi^\top) v \\ \Phi \Phi^\top \xi = \Phi \left\{ (\Lambda^2 + \mathbf{I}_r)^{-1/2} \Phi^\top v + \Lambda (\Lambda^2 + \mathbf{I}_r)^{-1/2} \Psi^\top G(v) \right\}. \end{cases}$$

Equation (10) separates  $\xi$  into two parts: one in the column space of  $\Phi$  and another in its orthogonal complement. Suppose we have a basis for the complement space  $\Phi_\perp = [\phi_{r+1}, \phi_{r+2}, \dots]$ <sup>1</sup> such that  $[\Phi, \Phi_\perp]$  form a complete orthonormal basis for  $\mathbb{R}^n$ . We can solve the nonlinear system of equations (10) by defining

$$v_\perp = (\Phi_\perp)^\top v, \quad v_r = \Phi^\top v, \quad v = \Phi_\perp v_\perp + \Phi v_r,$$

setting the components in the orthogonal complement of  $\Phi$  to

$$(11) \quad \Phi_\perp v_\perp = (\mathbf{I}_n - \Phi \Phi^\top) \xi,$$

and then solving the  $r$ -dimensional optimization problem

$$(12) \quad v_r = \arg \min_{v'_r} \left\| (\Lambda^2 + \mathbf{I}_r)^{-1/2} v'_r + \Lambda (\Lambda^2 + \mathbf{I}_r)^{-1/2} \Psi^\top G(\Phi_\perp v_\perp + \Phi v'_r) - \Phi^\top \xi \right\|^2.$$

Equations (11) and (12) replace the  $n$ -dimensional optimization problem in (5). In addition, at Step 7 of Algorithm 1, we need to calculate the expression  $w(v)$  in (7). First, note that (9) implies

$$\begin{aligned} \tilde{Q}^\top \nabla H(v) &= \Phi(\Lambda^2 + \mathbf{I})^{-\frac{1}{2}} \Phi^\top + (\mathbf{I} - \Phi \Phi^\top) + \Phi \Lambda (\Lambda^2 + \mathbf{I})^{-\frac{1}{2}} \Psi^\top \nabla G(v) \\ &= \mathbf{I} + \Phi \left[ (\Lambda^2 + \mathbf{I})^{-\frac{1}{2}} \Phi^\top - \Phi^\top + \Lambda (\Lambda^2 + \mathbf{I})^{-\frac{1}{2}} \Psi^\top \nabla G(v) \right]. \end{aligned}$$

---

<sup>1</sup>We do not actually compute  $\Phi_\perp$ . It is used to represent the complement space mathematically.



Hence, the determinant term is given by

$$\begin{aligned}
(13) \quad \left| \det \left( \tilde{Q}^\top \nabla H(v) \right) \right| &= \left| \det \left( \mathbf{I} + \Phi \left[ (\Lambda^2 + \mathbf{I})^{-\frac{1}{2}} \Phi^\top - \Phi^\top + \Lambda (\Lambda^2 + \mathbf{I})^{-\frac{1}{2}} \Psi^\top \nabla G(v) \right] \right) \right| \\
&= \left| \det \left( \mathbf{I} + \left[ (\Lambda^2 + \mathbf{I})^{-\frac{1}{2}} \Phi^\top - \Phi^\top + \Lambda (\Lambda^2 + \mathbf{I})^{-\frac{1}{2}} \Psi^\top \nabla G(v) \right] \Phi \right) \right| \\
&= \left| \det \left( \mathbf{I} + (\Lambda^2 + \mathbf{I})^{-\frac{1}{2}} - \mathbf{I} + \Lambda (\Lambda^2 + \mathbf{I})^{-\frac{1}{2}} \Psi^\top \nabla G(v) \Phi \right) \right| \\
&= \left| \det(\Lambda^2 + \mathbf{I})^{-\frac{1}{2}} \right| \left| \det(\mathbf{I} + \Lambda \Psi^\top \nabla G(v) \Phi) \right|
\end{aligned}$$

where in line 2 above we use Sylvester’s determinant identity, and in line 3 we use the fact that  $\Phi^\top \Phi = \mathbf{I}$ . This formulation replaces the  $n \times n$  determinant calculation with one of size  $r \times r$ .

To summarize, we presented an implementation of RTO that avoids the QR factorization of  $\nabla H(v_{\text{MAP}})$  and opts to store the SVD of the smaller matrix  $\nabla G(v_{\text{MAP}})$ . As a result, we reduce the size of the optimization problem and reduce the size of the matrix determinant calculation for each proposal. The new scalable implementation reduces the computational complexity of taking a step in MCMC from  $O(n^3)$  to  $O(nrm)$ . This is advantageous when the size of the parameter vector is much larger than the number of observations. This implementation is outlined in Algorithm 2.

---

**Algorithm 2** Scalable implementation of RTO–MH

---

- 1: Find  $v_{\text{MAP}}$  using (3).
  - 2: Determine the Jacobian matrix of the forward model,  $\nabla G(v_{\text{MAP}})$ .
  - 3: Compute  $\Psi$ ,  $\Lambda$  and  $\Phi$ , which is the SVD of  $\nabla G(v_{\text{MAP}})$ .
  - 4: **for**  $i = 1, \dots, n_{\text{samps}}$  **do** in parallel
  - 5:     Sample  $\xi^{(i)}$  from an  $n$ -dimensional standard normal distribution.
  - 6:     Solve for a proposal sample  $v_{\text{prop}}^{(i)} = \Phi_\perp v_\perp + \Phi v_r$  using (11) and (12).
  - 7:     Compute  $w(v_{\text{prop}}^{(i)})$  from (7) using the determinant from (13).
  - 8: Set  $v^{(0)} = v_{\text{MAP}}$ .
  - 9: **for**  $i = 1, \dots, n_{\text{samps}}$  **do** in series
  - 10:     Sample  $t$  from a uniform distribution on  $[0, 1]$ .
  - 11:     **if**  $t < w(v_{\text{prop}}^{(i)}) / w(v^{(i-1)})$  **then**
  - 12:          $v^{(i)} = v_{\text{prop}}^{(i)}$ .
  - 13:     **else**
  - 14:          $v^{(i)} = v^{(i-1)}$ .
- 

*Remark 2.* We can truncate the rank of the SVD in cases where data is abundant, i.e., when  $y \in \mathbb{R}^m$  is a large vector. This will change RTO’s map and the resulting proposal distribution. Figure 2 shows the effect on RTO’s proposal of truncating the SVD, in a toy example with a nonlinear forward model and a standard normal prior. Truncation restricts the role of the data misfit term in the construction of the proposal distribution. As the rank  $r$  decreases, the proposal distribution becomes broader. In the extreme case, when the  $r$  is truncated to zero, RTO’s proposal reverts to the prior. Note, however, the non-Gaussianity of the proposal for  $r \geq 1$  in this nonlinear example.

**5. Dimension independence of RTO.** In numerical experiments (see Section 6 and [29]), we observe that the acceptance rate and the effective sample size (for a fixed number of MCMC iterations) of RTO is independent of the parameter dimension. In this section, we will justify this behavior by showing that RTO yields a valid MCMC proposal in the function space setting [27].

Suppose the parameter space is a separable Hilbert space  $\mathcal{H}$  and endowed with a Gaussian prior measure  $\mu_{\text{pr}}$  such that  $\mu_{\text{pr}}(\mathcal{H}) = 1$ . We denote the probability measure induced by the RTO mapping

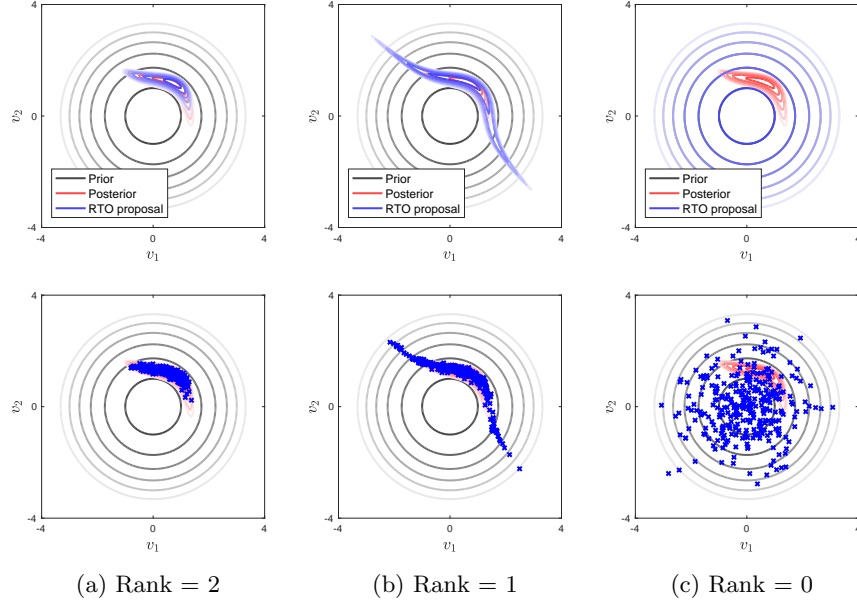


Fig. 2: Truncating the SVD in a two-dimensional toy example with a nonlinear forward model and standard normal prior. Top: contours of the prior, posterior and RTO’s proposal density. Bottom: contours of the prior and posterior densities, and samples from RTO’s proposal.

as  $\mu_{\text{RTO}}$ . The following theorem establishes conditions on  $\mu_{\text{RTO}}$  such that the MH algorithm using RTO as its independence proposal will be well defined on  $\mathcal{H}$ .

**THEOREM 3.** *Suppose the target measure  $\mu_{\text{tar}}$  is equivalent to the prior measure  $\mu_{\text{pr}}$ , i.e.,  $\mu_{\text{tar}} \sim \mu_{\text{pr}}$ . If the Radon–Nikodym derivative of the target measure with respect to the RTO measure,*

$$(14) \quad \omega(u) := \frac{d\mu_{\text{tar}}}{d\mu_{\text{RTO}}}(u),$$

*is positive almost surely with respect to  $\mu_{\text{pr}}$ , then the acceptance probability of the MH algorithm using RTO as its independence proposal is positive almost surely with respect to  $\mu_{\text{pr}} \times \mu_{\text{pr}}$ .*

*Proof.* The proof can be viewed as a special case of Theorem 5.1 in [27]. Let  $q(u, du')$  denote the probability measure of the MH proposal starting from the point  $u$ . We can define the following pair of measures on  $\mathcal{H} \times \mathcal{H}$ :

$$\begin{aligned} \nu(du, du') &:= q(u, du') \mu_{\text{tar}}(du) \\ \nu^\perp(du, du') &:= q(u', du) \mu_{\text{tar}}(du'). \end{aligned}$$

The acceptance probability of MH is then given by the Radon–Nikodym derivative

$$\alpha(u, u') = \min \left( 1, \frac{d\nu^\perp}{d\nu}(u, u') \right).$$

Since RTO is an independent proposal, the resulting MH proposal measure becomes

$$q(u, du') = \mu_{\text{RTO}}(du'),$$

and the pair of transition measures become

$$\begin{aligned}\nu(du, du') &= \mu_{\text{RTO}}(du') \mu_{\text{tar}}(du) \\ \nu^\perp(du, du') &= \mu_{\text{RTO}}(du) \mu_{\text{tar}}(du'),\end{aligned}$$

This way, the acceptance probability can be expressed as

$$\alpha(u, u') = \min \left( 1, \frac{d\mu_{\text{tar}}(u')}{d\mu_{\text{RTO}}(u)} \right) = \min \left( 1, \frac{\omega(u')}{\omega(u)} \right).$$

If and only if  $\omega(u)$  is positive  $\mu_{\text{pr}}$ -almost surely, the acceptance probability is positive  $\mu_{\text{pr}} \times \mu_{\text{pr}}$ -almost surely.  $\square$

If the acceptance probability is positive almost surely with respect to  $\mu_{\text{pr}} \times \mu_{\text{pr}}$ , the posterior is invariant for the Markov chain of the resulting MH algorithm. Hence, as shown in [27], the algorithm is well-posed in function space and has sampling performance independent of the parameter discretization dimension.

In the rest of this section, we will focus on establishing sufficient conditions for the Radon–Nikodym derivative  $\omega(u)$  to be positive  $\mu_{\text{pr}}$ -almost surely. We outline the broad steps of the derivation as follows. In Section 5.1, we derive the unwhitened mapping for RTO in a finite-dimensional (discrete) setting. Because the unwhitened prior corresponds to a discretized Gaussian process, we can naturally generalize RTO to an infinite-dimensional Hilbert space setting in Section 5.2. Motivated by Section 4, we introduce a particular rank- $r$  projection operator  $P : \mathcal{H} \rightarrow \mathcal{H}$  and use it to define RTO’s inverse map. In Section 5.3, we derive RTO’s proposal measure as the pullback of the prior measure through this inverse map. This construction allows us to establish conditions ensuring that  $\omega(u)$  is positive  $\mu_{\text{pr}}$ -almost surely.

**5.1. Unwhitened mapping in finite dimensions.** In this subsection, we derive the unwhitened mapping for RTO in a finite-dimensional setting. In Figure 3, we specify the relationship between four finite-dimensional random variables:  $u$ ,  $v$ ,  $\xi$ , and  $\zeta$ , where  $\zeta$  is a newly defined random variable distributed according to the prior. Note that here we use  $u$  and  $v$  to denote random variables distributed according to the unwhitened and whitened *proposal* distributions, respectively, rather than the corresponding posterior distributions. Recall that  $S_{\text{pr}}$  and  $m_{\text{pr}}$  were defined in Section 2.1.

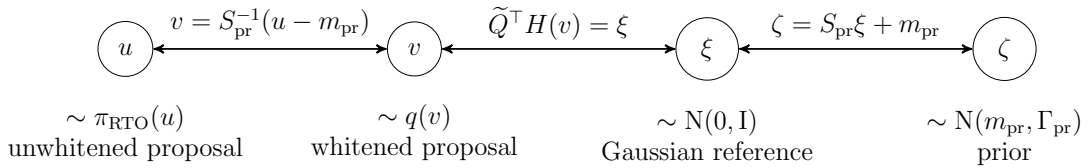


Fig. 3: Relationship between four random variables.

The RTO mapping (10) in the unwhitened coordinates takes the form

$$\begin{aligned}S_{\text{pr}}^{-1}(\zeta - m_{\text{pr}}) &= \Phi \left[ (\Lambda^2 + \mathbf{I})^{-1/2} \Phi^\top S_{\text{pr}}^{-1}(u - m_{\text{pr}}) + \Lambda(\Lambda^2 + \mathbf{I})^{-1/2} \Psi^\top S_{\text{obs}}^{-1}(F(u) - y) \right] \\ &\quad + (\mathbf{I} - \Phi \Phi^\top) S_{\text{pr}}^{-1}(u - m_{\text{pr}}).\end{aligned}$$

Defining the oblique projectors

$$P := S_{\text{pr}} \Phi \Phi^\top S_{\text{pr}}^{-1}, \quad \mathbf{I} - P = S_{\text{pr}} (\mathbf{I} - \Phi \Phi^\top) S_{\text{pr}}^{-1},$$

and multiplying both sides of the above equation by  $S_{\text{pr}}$ , we can express the unwhitened RTO mapping in the following split form:

$$(15) \quad \begin{cases} (\mathbf{I} - P)(\zeta - m_{\text{pr}}) &= (\mathbf{I} - P)(u - m_{\text{pr}}) \\ P(\zeta - m_{\text{pr}}) &= S_{\text{pr}}\Phi\Theta(u), \end{cases}$$

where

$$(16) \quad \Theta(u) = (\Lambda^2 + \mathbf{I})^{-1/2}\Phi^\top S_{\text{pr}}^{-1}(u - m_{\text{pr}}) + \Lambda(\Lambda^2 + \mathbf{I})^{-1/2}\Psi^\top S_{\text{obs}}^{-1}(F(u) - y),$$

is an affine transformation of the nonlinear forward model  $F$ .

Define the matrix  $\mathbb{R}^{n \times r} \ni \mathcal{X} := S_{\text{pr}}\Phi$  and let  $\chi_i \in \mathbb{R}^n$  be its columns. These columns  $\chi_i$  are orthonormal with respect to the  $\Gamma_{\text{pr}}^{-1}$ -inner product (i.e.,  $\langle \cdot, \cdot \rangle_{\Gamma_{\text{pr}}^{-1}}$ ).<sup>2</sup> Let us define a second matrix  $\mathcal{X}_\perp \in \mathbb{R}^{n \times (n-r)}$  such that the columns of  $[\mathcal{X} \ \mathcal{X}_\perp]$  form a complete orthonormal basis for  $\mathbb{R}^n$  with respect to the  $\Gamma_{\text{pr}}^{-1}$ -inner product. Then,  $P$  is the  $\Gamma_{\text{pr}}^{-1}$ -orthogonal projector that projects any vector onto the first  $r$  basis vectors (the columns of  $\mathcal{X}$ ). Now, let  $\langle \mathcal{X}, \cdot \rangle_{\Gamma_{\text{pr}}^{-1}} : \mathbb{R}^n \rightarrow \mathbb{R}^r$  denote the map that takes a vector and returns its coefficients in the  $(\chi_1, \dots, \chi_r)$  basis. Specifically, we define this map via inner products as:

$$\langle \mathcal{X}, \cdot \rangle_{\Gamma_{\text{pr}}^{-1}} = \begin{bmatrix} \langle \chi_1, \cdot \rangle_{\Gamma_{\text{pr}}^{-1}} \\ \langle \chi_2, \cdot \rangle_{\Gamma_{\text{pr}}^{-1}} \\ \vdots \\ \langle \chi_r, \cdot \rangle_{\Gamma_{\text{pr}}^{-1}} \end{bmatrix}.$$

By this definition,  $\langle \mathcal{X}, u - m_{\text{pr}} \rangle_{\Gamma_{\text{pr}}^{-1}}$  is a vector of size  $r \times 1$ . Let  $\langle \mathcal{X}_\perp, \cdot \rangle_{\Gamma_{\text{pr}}^{-1}}$  be defined in a similar manner.

The mapping (15) can thus be rewritten in terms of these coefficients:

$$(17) \quad \begin{cases} \langle \mathcal{X}_\perp, \zeta - m_{\text{pr}} \rangle_{\Gamma_{\text{pr}}^{-1}} &= \langle \mathcal{X}_\perp, u - m_{\text{pr}} \rangle_{\Gamma_{\text{pr}}^{-1}} \\ \langle \mathcal{X}, \zeta - m_{\text{pr}} \rangle_{\Gamma_{\text{pr}}^{-1}} &= \Theta(u) \end{cases},$$

where the function  $\Theta(u)$  can be correspondingly expressed as

$$\Theta(u) = (\Lambda^2 + \mathbf{I})^{-1/2} \langle \mathcal{X}, u - m_{\text{pr}} \rangle_{\Gamma_{\text{pr}}^{-1}} + \Lambda(\Lambda^2 + \mathbf{I})^{-1/2} \Psi^\top S_{\text{obs}}^{-1}(F(u) - y).$$

Note that the two equations (15) and (17) are equivalent. They both describe RTO's mapping in finite dimensions: the first in terms of the vectors in the range and null space of  $P$ , and the second in terms of coefficients in our chosen basis (the columns of  $\mathcal{X}$  and  $\mathcal{X}_\perp$ ).

**5.2. RTO mapping in function space.** In this section, we define an RTO mapping in function space. Until now we worked with finite dimensional random vectors  $u \in \mathbb{R}^n$  and  $\zeta \in \mathbb{R}^n$ . Here and in Section 5.3, we will use the same symbols  $u$  and  $\zeta$  to denote random variables taking values in a separable Hilbert space  $\mathcal{H}$ . Let  $\zeta$  be distributed according to the prior, which we assume to be a Gaussian measure  $\mu_{\text{pr}}$  on  $\mathcal{H}$  with trace-class covariance operator  $\Gamma_{\text{pr}}$  and mean function  $m_{\text{pr}}$ . (In general, we will use the same notation in the function space setting as we do in the finite dimensional setting, except that we will now use  $\Gamma_{\text{pr}}^{1/2}$  to denote the square root of the prior covariance operator. This overloading of notation is intended to preserve interpretability.)

Recall that the Cameron–Martin space associated with  $\mu_{\text{pr}}$ ,  $\mathcal{H}_{\text{CM}} = \Gamma_{\text{pr}}^{1/2} \mathcal{H} \subset \mathcal{H}$ , is equipped with the inner product

$$\langle a, b \rangle_{\mathcal{H}_{\text{CM}}} = \langle a, b \rangle_{\Gamma_{\text{pr}}^{-1}} = \left\langle \Gamma_{\text{pr}}^{-1/2} a, \Gamma_{\text{pr}}^{-1/2} b \right\rangle_{\mathcal{H}},$$

<sup>2</sup>We use the notation  $\langle a, b \rangle_C := a^\top C b$  for any  $a, b \in \mathbb{R}^n$  and symmetric positive definite  $C \in \mathbb{R}^{n \times n}$ .

for any  $a, b \in \mathcal{H}_{\text{CM}}$ . Suppose that we are given a finite set of orthonormal functions  $\{\phi_i \in \mathcal{H}, i = 1, \dots, r\}$ , and also suppose that each  $\phi_i \in \mathcal{H}_{\text{CM}}$ . Let  $\chi_i \in \mathcal{H}_{\text{CM}}$  be defined as  $\chi_i := \Gamma_{\text{pr}}^{1/2} \phi_i$ . Then, by construction,  $\chi_i$  are orthonormal with respect to the  $\mathcal{H}_{\text{CM}}$ -inner product. In addition, since  $\phi_i \in \mathcal{H}_{\text{CM}}$ , we have that  $\chi_i \in \Gamma_{\text{pr}}^{1/2} \mathcal{H}_{\text{CM}}$ . We can overwrite the definition of the  $\mathcal{H}_{\text{CM}}$ -inner product, typically only used for elements in the Cameron–Martin space, for inputs of type  $\Gamma_{\text{pr}}^{1/2} \mathcal{H}_{\text{CM}} \times \mathcal{H}$ . Namely, for any  $c \in \Gamma_{\text{pr}}^{1/2} \mathcal{H}_{\text{CM}}$  and  $d \in \mathcal{H}$ , we write

$$\langle c, d \rangle_{\mathcal{H}_{\text{CM}}} = \left\langle \Gamma_{\text{pr}}^{-1/2} c, \Gamma_{\text{pr}}^{1/2} d \right\rangle_{\mathcal{H}_{\text{CM}}},$$

where the inner product on the right is defined in the usual manner (i.e., between two elements in  $\mathcal{H}_{\text{CM}}$ ). In other words, we are treating  $\Gamma_{\text{pr}}^{1/2} \mathcal{H}_{\text{CM}}$  as the dual of  $\mathcal{H}$  with respect to the  $\mathcal{H}_{\text{CM}}$ -inner product. This allows us to compute  $\mathcal{H}_{\text{CM}}$ -inner products of  $\chi_i$  with any function in  $\mathcal{H}$ .

Let us define the linear subspace  $W \subset \mathcal{H}_{\text{CM}}$  to be

$$W := \overline{\text{span}}\{\chi_i\}_{i=1}^r,$$

where  $\overline{\text{span}}$  denotes the closure of the span. Analogous to the finite-dimensional case, we define the operators  $\mathcal{X}(\cdot) : \mathbb{R}^r \rightarrow W$  and  $\langle \mathcal{X}, \cdot \rangle_{\mathcal{H}_{\text{CM}}} : \mathcal{H} \rightarrow \mathbb{R}^r$  as

$$\mathcal{X}(c) := \sum_{i=1}^r c_i \chi_i \quad \langle \mathcal{X}, a \rangle_{\mathcal{H}_{\text{CM}}} := \begin{bmatrix} \langle \chi_1, a \rangle_{\mathcal{H}_{\text{CM}}} \\ \langle \chi_2, a \rangle_{\mathcal{H}_{\text{CM}}} \\ \vdots \\ \langle \chi_r, a \rangle_{\mathcal{H}_{\text{CM}}} \end{bmatrix}$$

for any function  $a \in \mathcal{H}$  and any vector of coefficients  $c \in \mathbb{R}^r$ . Let the projection operator  $P : \mathcal{H} \rightarrow W$  be defined as

$$P a := \sum_{i=1}^r \langle \chi_i, a \rangle_{\mathcal{H}_{\text{CM}}} \chi_i = \mathcal{X}(\langle \mathcal{X}, a \rangle_{\mathcal{H}_{\text{CM}}})$$

for any  $a \in \mathcal{H}$  and let the subspace  $W^\perp$  be defined as

$$W^\perp := \{a \in \mathcal{H} \mid P a = 0\} = \{a \in \mathcal{H} \mid \langle \chi_i, a \rangle_{\mathcal{H}_{\text{CM}}} = 0 \text{ for all } i = 1, \dots, r\}.$$

Then, one can show that  $P$  maps  $\mathcal{H} \rightarrow W$  and  $(I - P)$  maps  $\mathcal{H} \rightarrow W^\perp$ . Any function  $a \in \mathcal{H}$  can be uniquely split into two parts using the projection  $P$ .

$$a = \underbrace{P a}_{\in W} + \underbrace{(I - P) a}_{\in W^\perp}.$$

Now, the infinite-dimensional analogue to RTO's unwhitened mapping (15) and (17) between the random variables  $u \in \mathcal{H}$  and  $\zeta \in \mathcal{H}$  can be expressed as:

$$(18) \quad \begin{cases} (I - P)(\zeta - m_{\text{pr}}) &= (I - P)(u - m_{\text{pr}}) \\ P(\zeta - m_{\text{pr}}) &= \mathcal{X}\Theta(u) \end{cases},$$

where

$$\Theta(u) = (\Lambda^2 + I)^{-1/2} \langle \mathcal{X}, u - m_{\text{pr}} \rangle_{\mathcal{H}_{\text{CM}}} + \Lambda(\Lambda^2 + I)^{-1/2} \Psi^\top S_{\text{obs}}^{-1} (F(u) - y).$$

*Remark 4.* Above we assumed that  $\chi_i$  are in  $\Gamma_{\text{pr}}^{1/2} \mathcal{H}_{\text{CM}}$  or, in other words, that  $\phi_i$  are in  $\mathcal{H}_{\text{CM}}$ . This is true when we obtain  $\phi_i$  from the linearization of the forward model evaluated at the MAP. Note that

$$\Phi \Lambda^2 \Phi^\top = \nabla G(v_{\text{MAP}})^\top \nabla G(v_{\text{MAP}}) = \Gamma_{\text{pr}}^{1/2} \nabla F(u_{\text{MAP}})^\top \Gamma_{\text{obs}}^{-1} \nabla F(u_{\text{MAP}}) \Gamma_{\text{pr}}^{1/2}.$$

The operator  $\nabla F(u_{\text{MAP}})^\top \Gamma_{\text{obs}}^{-1} \nabla F(u_{\text{MAP}})$  has rank  $r$  with  $r \leq m$ . In other words, there are a finite collection of functions  $\{\phi_i\}$  satisfying

$$\Gamma_{\text{pr}}^{\frac{1}{2}} \nabla F(u_{\text{MAP}})^\top \Gamma_{\text{obs}}^{-1} \nabla F(u_{\text{MAP}}) \Gamma_{\text{pr}}^{\frac{1}{2}} \phi_i = \lambda_i \phi_i, \quad i = 1, \dots, r.$$

We plug in  $\chi_i = \Gamma_{\text{pr}}^{\frac{1}{2}} \phi_i$  to see that the functions  $\chi_i$  are the eigenfunctions that satisfy

$$\Gamma_{\text{pr}} \nabla F(u_{\text{MAP}})^\top \Gamma_{\text{obs}}^{-1} \nabla F(u_{\text{MAP}}) \chi_i = \lambda_i \chi_i, \quad i = 1, \dots, r.$$

Since  $\nabla F(u_{\text{MAP}})^\top \Gamma_{\text{obs}}^{-1} \nabla F(u_{\text{MAP}})$  maps  $\mathcal{H} \rightarrow \mathcal{H}$ ,  $\nabla F(u_{\text{MAP}})^\top \Gamma_{\text{obs}}^{-1} \nabla F(u_{\text{MAP}}) \chi_i$  is in  $\mathcal{H}$  and the left-hand side of the equation above is in  $\Gamma_{\text{pr}} \mathcal{H}$ . Thus the right-hand side  $\lambda_i \chi_i$  is also in  $\Gamma_{\text{pr}} \mathcal{H}$ , meaning that we can apply the prior precision operator directly to the functions  $\chi_i$  and still obtain an element of  $\mathcal{H}$ . Hence  $\chi_i \in \Gamma_{\text{pr}} \mathcal{H} = \Gamma_{\text{pr}}^{\frac{1}{2}} \mathcal{H}_{\text{CM}}$  or, equivalently,  $\phi_i \in \mathcal{H}_{\text{CM}}$ .

**5.3. Equivalence of RTO's proposal and the prior.** With the function space analogue of RTO defined in the previous section, we will now prove that, under certain conditions, the proposal measure  $\pi_{\text{RTO}}$  is equivalent to the prior  $\mu_{\text{pr}}$ . This step is the key to showing that  $\omega(u)$  is positive  $\mu_{\text{pr}}$ -almost surely.

**THEOREM 5.** *Suppose that the prior  $\mu_{\text{pr}}$  is a non-degenerate Gaussian measure on  $\mathcal{H}$ , the random variable  $\zeta$  is distributed according to  $\mu_{\text{pr}}$ , the random variable  $u$  is defined through the mapping in (18), and for every  $b \in W^\perp$ , the mapping*

$$a \mapsto a + \Lambda \Psi^\top S_{\text{obs}}^{-1} (F(\mathcal{X}(a) + b) - y)$$

*is Lipschitz continuous, injective, and its inverse is Lipschitz continuous. Let  $\mu_{\text{RTO}}$  be the measure induced by  $u$ . Then  $\mu_{\text{RTO}}$  is equivalent to  $\mu_{\text{pr}}$ .*

*Proof.* Previously, we have used the notation  $u \in \mathcal{H}$  to define a random function taking values in  $\mathcal{H}$ . In this proof only, we will employ the probability triplet  $(\Omega, \mathcal{F}, \mathbb{P})$  and switch to describing the random function more formally as the map  $u : \Omega \rightarrow \mathcal{H}$ . We assume that the measurable space  $(\Omega, \mathcal{F})$  is a Radon space. Let the random variable  $\zeta$  be distributed according to the prior measure and  $u$  be distributed according to RTO's proposal measure. Without loss of generality, let the prior mean be zero. Define the following four random variables:

$$\begin{aligned} \zeta_r : \Omega &\rightarrow \mathbb{R}^r & \zeta_r &:= \langle \mathcal{X}, \zeta(\cdot) \rangle_{\mathcal{H}_{\text{CM}}}, \\ u_r : \Omega &\rightarrow \mathbb{R}^r & u_r &:= \langle \mathcal{X}, u(\cdot) \rangle_{\mathcal{H}_{\text{CM}}}, \\ \zeta_\perp : \Omega &\rightarrow W^\perp & \zeta_\perp &:= (\text{I} - P) \circ \zeta, \\ u_\perp : \Omega &\rightarrow W^\perp & u_\perp &:= (\text{I} - P) \circ u. \end{aligned}$$

We can concisely summarize RTO's mapping in (18) as

$$\begin{cases} u_\perp &= \zeta_\perp \\ \mathfrak{S}(u_r; u_\perp) &= \zeta_r \end{cases}$$

where for any  $b \in W^\perp$ , the expression  $\mathfrak{S}(\cdot; b)$  maps  $\mathbb{R}^r \rightarrow \mathbb{R}^r$ , and in addition for any  $a \in \mathbb{R}^r$ , the term  $\mathfrak{S}(a; b)$  is defined as

$$\mathfrak{S}(a; b) := (\Lambda^2 + \text{I})^{-1/2} a + \Lambda (\Lambda^2 + \text{I})^{-1/2} \Psi^\top S_{\text{obs}}^{-1} (F(\mathcal{X}(a) + b) - y).$$

The relationships between the six random variables  $u$ ,  $u_r$ ,  $u_\perp$ ,  $\zeta$ ,  $\zeta_r$ , and  $\zeta_\perp$ , and the spaces they map to and from, are depicted in Figure 4.

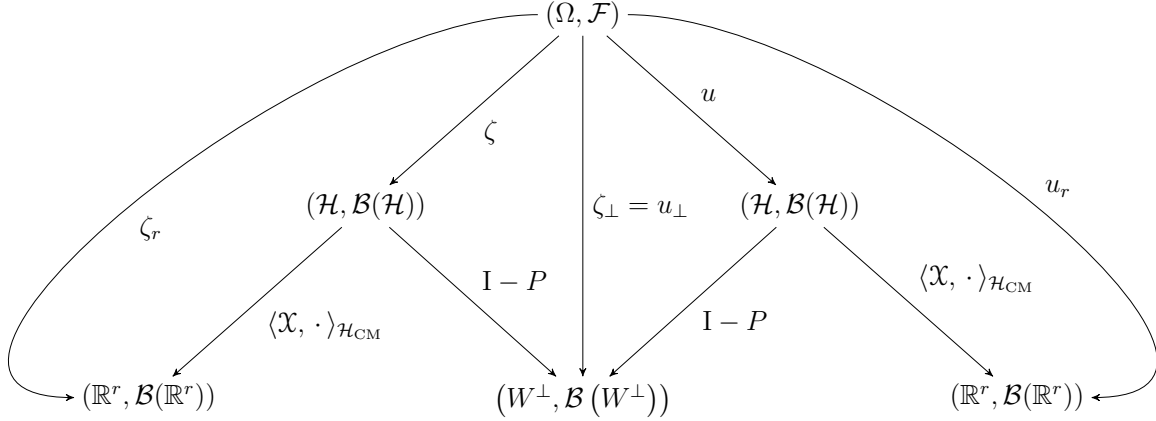


Fig. 4: Relationship between the six random variables and the spaces they map to and from.  $\mathcal{B}(W)$  denotes the Borel  $\sigma$ -algebra of  $W$  for any space  $W$ .

Now, let the notation  $\mathbb{P}^u$  denote the push-forward measure of  $\mathbb{P}$  through  $u$

$$\mathbb{P}^u := u_{\#}\mathbb{P} = \mathbb{P}(u^{-1}(\cdot)) = \mathbb{P}(u \in \cdot)$$

Using this notation, we have that

$$\mu_{\text{pr}} := \mathbb{P}^{\zeta} \qquad \mu_{\text{RTO}} := \mathbb{P}^u.$$

We can use the random variable  $\zeta_{\perp}$  (which is exactly the same as the random variable  $u_{\perp}$ ) to define a regular conditional probability  $\nu : W^{\perp} \times \mathcal{F} \rightarrow [0, 1]$  where for any  $A \in \mathcal{F}$  and  $b \in W^{\perp}$ ,

$$\nu : (b, A) \rightarrow \nu(b, A) = \mathbb{P}(A \mid \zeta_{\perp} = b).$$

By definition, the regular conditional probability  $\nu$  satisfies the following three properties

1. For all  $b \in W^{\perp}$ ,  $\nu(b, \cdot)$  is a valid probability measure on  $\mathcal{F}$ .
2. For all  $A \in \mathcal{F}$ ,  $\nu(\cdot, A)$  is a measurable function.
3. For all  $A \in \mathcal{F}$  and  $B \in \mathcal{B}(W^{\perp})$ ,

$$\mathbb{P}(A \cap \zeta_{\perp}^{-1}(B)) = \int_B \nu(x, A) \mathbb{P}^{\zeta_{\perp}}(dx).$$

Given a fixed  $b \in W^{\perp}$ , consider the following two measures

$$\mathbb{P}(\zeta_r \in \cdot \mid \zeta_{\perp} = b) = \nu(b, \zeta_r^{-1}(\cdot)) : \mathcal{B}(\mathbb{R}^r) \rightarrow [0, 1]$$

$$\mathbb{P}(u_r \in \cdot \mid \zeta_{\perp} = b) = \nu(b, u_r^{-1}(\cdot)) : \mathcal{B}(\mathbb{R}^r) \rightarrow [0, 1]$$

These are the measures of  $\zeta_r$  and  $u_r$  conditioned on  $\zeta_{\perp} = b$ . They are measures on  $\mathbb{R}^r$ . We will use their densities with respect to the Lebesgue measure on  $\mathbb{R}^r$  to find the Radon–Nikodym derivative between the two. Note that the measure  $\nu(b, \zeta_r^{-1}(\cdot))$  is the measure of a finite number of directions,  $\zeta_r$ , of the prior (a nondegenerate Gaussian measure) conditioned on a particular value,  $\zeta_{\perp} = b$ , of its orthogonal directions. The two random variables  $\zeta_r$  and  $\zeta_{\perp}$  are independent (see Proposition 1.26 of [23]). Hence, the measure  $\nu(b, \zeta_r^{-1}(\cdot))$  is equivalent to the law of  $\zeta_r$  and is a non-degenerate Gaussian measure. Let  $\pi_{\zeta_r|b}$  denote its probability density function. Then for any  $A \in \mathcal{B}(\mathbb{R}^r)$ ,

$$\nu(b, \zeta_r^{-1}(A)) = \int_A \nu(b, \zeta_r^{-1}(dx)) = \int_A \pi_{\zeta_r|b}(x) dx$$



and likewise for any  $A \in \mathcal{B}(\mathbb{R}^r)$ ,

$$\begin{aligned}
\mathbb{P}(u_r \in A \mid \zeta_\perp = b) &= \nu(b, u_r^{-1}(A)) = \nu(b, \zeta_r^{-1} \circ \mathfrak{S}(A; b)) \\
&= \int_{\mathfrak{S}(A; b)} \pi_{\zeta_r|b}(x) dx \\
&= \int_A \pi_{\zeta_r|b} \circ \mathfrak{S}(x; b) |\det \nabla \mathfrak{S}(x; b)| dx \\
&= \int_A \frac{\pi_{\zeta_r|b} \circ \mathfrak{S}(x; b)}{\pi_{\zeta_r|b}(x)} |\det \nabla \mathfrak{S}(x; b)| \pi_{\zeta_r|b}(x) dx \\
&= \int_A \frac{\pi_{\zeta_r|b} \circ \mathfrak{S}(x; b)}{\pi_{\zeta_r|b}(x)} |\det \nabla \mathfrak{S}(x; b)| \nu(b, \zeta_r^{-1}(dx)) \\
&= \int_A \mathfrak{R}(x; b) \nu(b, \zeta_r^{-1}(dx))
\end{aligned}$$

where for any  $a \in \mathbb{R}^r$  and  $b \in W^\perp$ , the expression  $\mathfrak{R}(a; b)$  is

$$\mathfrak{R}(a; b) := \frac{\pi_{\zeta_r|b} \circ \mathfrak{S}(a; b)}{\pi_{\zeta_r|b}(a)} |\det \nabla \mathfrak{S}(a; b)|.$$

The change of variables for the integration uses the fact that  $\mathfrak{S}(\cdot; b)$  is Lipschitz continuous and injective, and that its inverse is Lipschitz continuous. Note that for almost all  $b \in W^\perp$  and  $a \in \mathbb{R}^r$ , the expression  $\mathfrak{R}(a; b)$  is positive. Now, we find the Radon–Nikodym derivative of the distribution of  $u$  with respect to the distribution of  $\zeta$ . For any  $A \in \mathcal{B}(\mathcal{H})$  and  $x \in W^\perp$ , let

$$A_r(x) := \{u_r \in \mathbb{R}^r \mid \mathcal{X}(u_r) + x \in A\}.$$

Then, for any  $A \in \mathcal{B}(\mathcal{H})$ ,

$$\begin{aligned}
\mathbb{P}^u(A) &= \mathbb{P}(\{u \in A\} \cap \{u_\perp \in W^\perp\}) = \int_{W^\perp} \nu(x, u^{-1}(A)) \mathbb{P}^{u_\perp}(dx) \\
&= \int_{W^\perp} \nu(x, u_r^{-1}(A_r(x))) \mathbb{P}^{u_\perp}(dx) \\
&= \int_{W^\perp} \int_{A_r(x)} \mathfrak{R}(y; x) \nu(x, \zeta_r^{-1}(dy)) \mathbb{P}^{\zeta_\perp}(dx).
\end{aligned}$$

Using the change of variables  $x = (\mathbf{I} - P)z$  and  $y = \langle \mathcal{X}, z \rangle_{\mathcal{H}_{\text{CM}}}$  for some  $z \in \mathcal{H}$ , we have that

$$\mathbb{P}^u(A) = \int_A \mathfrak{R}(\langle \mathcal{X}, z \rangle_{\mathcal{H}_{\text{CM}}}; (\mathbf{I} - P)z) \mathbb{P}^\zeta(dz).$$

In other words, the Radon–Nikodym derivative is

$$\frac{d\mu_{\text{RTO}}}{d\mu_{\text{pr}}}(z) = \mathfrak{R}(\langle \mathcal{X}, z \rangle_{\mathcal{H}_{\text{CM}}}; (\mathbf{I} - P)z).$$

which is positive almost everywhere. This implies that  $\mu_{\text{RTO}}$  is equivalent to  $\mu_{\text{pr}}$  and concludes the proof.  $\square$

**COROLLARY 6.** *Under the assumptions of Theorem 5, the Radon–Nikodym derivative of the target measure with respect to the RTO measure*

$$\omega(u) = \frac{d\mu_{\text{tar}}}{d\mu_{\text{RTO}}}(u),$$

*is  $\mu_{\text{pr}}$ -almost surely positive.*

*Proof.* This result directly follows from Theorem 5 and  $\mu_{\text{pr}} \sim \mu_{\text{tar}}$ .  $\square$

As a result, RTO is well defined on function space (given the conditions in Theorem 5); hence, refining the parameter discretization in a discrete setting should not asymptotically diminish RTO–MH’s sampling efficiency.

**6. Numerical example: elliptic PDE.** The previous section provided a theoretical argument for RTO’s dimension independence. This section numerically explores the factors that influence its sampling performance, using a simple elliptic PDE inverse problem. We describe the setup of the test case (Section 6.1) and then explore the effects of parameter dimension (Section 6.2) and observational noise (Section 6.3). We conclude by comparing the performances of RTO and pCN (Section 6.4).

**6.1. Problem setup.** The diffusion equation is used to model the spatial distribution of many physical quantities, such as temperature, electrostatic potential, or pressure in porous media. We consider the following stationary diffusion equation,

$$-\frac{d}{dx} \left( \kappa(x) \frac{dp(x)}{dx} \right) = f(x), \quad 0 < x < 1,$$

with boundary conditions

$$\kappa(0) \frac{dp(0)}{dx} = -1, \quad p(1) = 1,$$

and source term  $f$ . The diffusion coefficient  $\kappa$  is endowed with a log-normal prior distribution. In particular,  $\log \kappa$  is a Gaussian process with a Laplace-like differential operator as its precision operator. After discretization on a uniform grid with  $n$  nodes,  $\kappa$  is thus specified as

$$\kappa = 1.5 \exp \left( \Gamma_{\text{pr}}^{\frac{1}{2}} v \right) + 0.1 \quad \Gamma_{\text{pr}}^{-\frac{1}{2}} = \sqrt{n} \begin{bmatrix} \sqrt{n} & & & & \sqrt{n} \\ -1 & 1 & & & \\ & -1 & 1 & & \\ & & \ddots & \ddots & \\ & & & -1 & 1 \end{bmatrix}$$

where  $v \in \mathbb{R}^n$  is a vector of independent standard normals and we have abused notation so that  $\kappa \in \mathbb{R}^n$  above as well. For any realization of  $\kappa$ , the equation is solved numerically using finite differences. Derivatives of the potential field  $p$  with respect to  $\kappa$  are evaluated using adjoint codes. For the inverse problem, we suppose that the potential field is observed, with additive Gaussian noise, at nine equally-spaced points along the domain. Our goal is to condition the field  $\kappa$  on these observations. We generate synthetic data using a mesh size of 151, which does not correspond to any mesh size used in solving the inverse problem. The “true” diffusion coefficient, source term, potential field, and data are depicted in Figure 5. For the experiments below, all RTO runs are performed serially, although in practice the most expensive part of RTO—generating proposal samples—can be run embarrassingly parallel.

**6.2. Influence of parameter dimension.** In our first experiment, we solve the Bayesian inverse problem using RTO for a series of parameter dimensions ranging from  $n = 41$  to  $n = 10241$ . We fix the observational noise standard deviation to  $10^{-5}$  and, at each parameter dimension, run an MCMC chain of 5000 steps. The chains are started at the posterior mode. As shown in Figure 6, the posterior distributions obtained for the different discretizations match quite closely. As shown in Table 2, the acceptance rate and effective sample size (ESS) are both high and essentially constant with respect to parameter dimension. (We report the median ESS over all components of the  $n$ -dimensional chain.) These results provide an empirical demonstration of RTO’s dimension independence, meaning that the number of MCMC steps required to obtain a single effectively independent sample is independent of  $n$ .

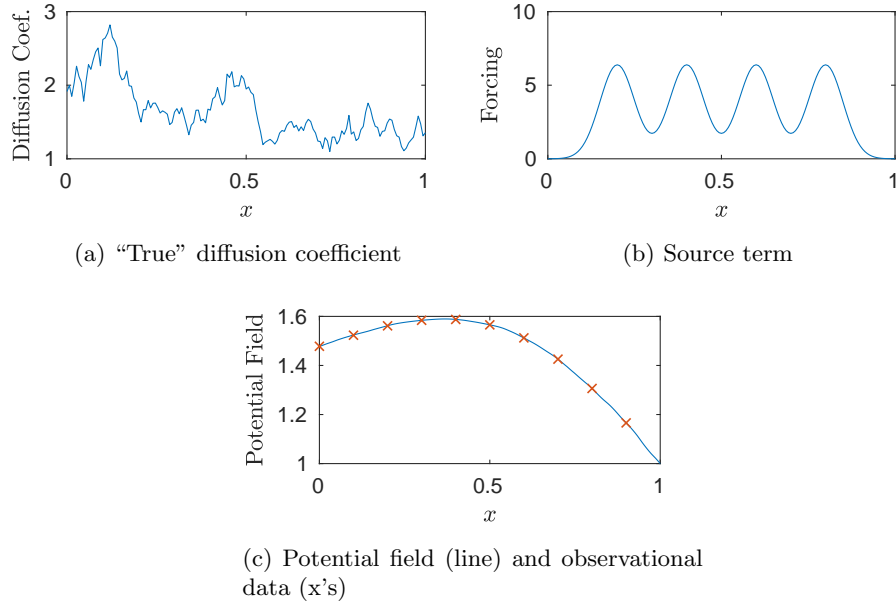


Fig. 5: Elliptic PDE problem setup.

The number of optimization iterations in each MCMC step is also roughly constant in  $n$ . To solve each optimization problem, we use the nonlinear least-squares solver in MATLAB, provided with Jacobian-vector products. The solver uses a trust-region-reflective algorithm where each iteration approximately solves a large linear system using preconditioned conjugate gradients. We set the starting point for each sequence of optimization iterations to the posterior mode. The primary stopping criterion is a function tolerance (i.e., a lower bound on the change in the value of the objective) of  $10^{-6}$ . Figure 7 shows the CPU times needed to generate one (effectively) independent sample, to take one MCMC step, and to evaluate the forward model once. The slopes of all three lines coincide, meaning that it takes the same number of forward model evaluations to obtain a desired accuracy regardless of parameter dimension. The increased computational cost for higher dimensions is only caused by a more expensive forward model. This result means that in addition to the number of MCMC steps, the number of function evaluations required for one independent sample also does not change with parameter dimension. Therefore, the computational cost of RTO is only affected by the number of parameters through the cost of the forward model.

Table 2: Effective sample size (ESS), average acceptance rate, and average number of optimization iterations per step of RTO, with varying parameter dimension. MCMC chain length is 5000 steps.

Parameter Dim.	41	81	161	321	641	1281	2561	5121	10241
ESS	4268.9	4206.7	4307.1	4343.5	4544.8	4464.5	4523.3	4484.9	4532.2
Acceptance Rate	0.928	0.926	0.932	0.936	0.948	0.950	0.954	0.950	0.953
Opt. Iterations	170.74	209.12	273.03	324.04	357.76	307.50	198.81	165.06	142.25

**6.3. Influence of observational noise.** In our second experiment, we examine the effect of observational noise magnitude on the sampling efficiency of RTO. We fix the parameter dimension to

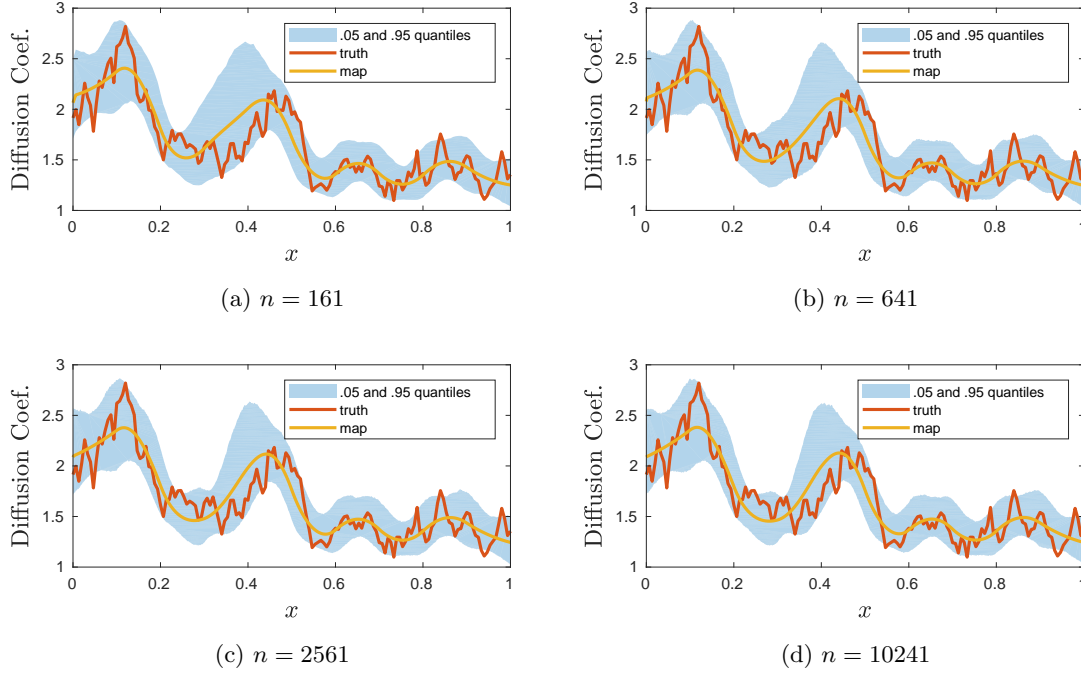


Fig. 6: Posterior distributions computed via RTO-MH with varying parameter dimension  $n$ . 90% marginal credibility intervals (blue shaded region), true diffusivity coefficient (red line), and MAP estimate (yellow line).

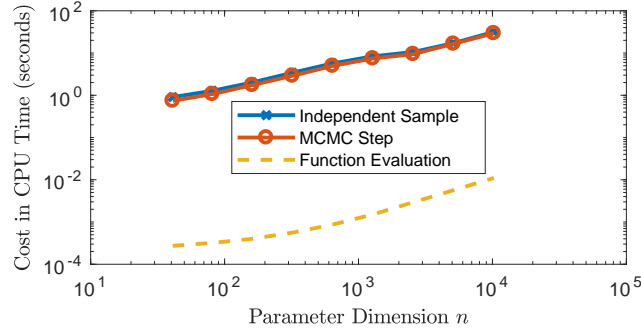


Fig. 7: Computational cost for elements of RTO, varying parameter dimension.

$n = 641$  and scan through observational noise standard deviations ranging from  $10^{-7}$  to  $10^0$ , which correspond to signal-to-noise ratios ranging from  $1.5 \times 10^7$  to  $1.5$ . Once again we run MCMC chains of length 5000. Changing the observational noise magnitude changes the posterior distribution, as shown in Figure 8. With extremely small observational noise, the probability mass of the posterior concentrates on the manifold where the parameter values yield outputs that exactly match the data. Generally, this collapse makes the posterior more difficult to simulate using most MCMC methods. In the case of RTO, it makes the optimization problems harder to solve. As shown in Table 3, even though the ESS and acceptance rate remain relatively constant with varying observational noise,

the number of optimization iterations required to obtain each sample increases as the observational noise becomes very small. Thus, as the observational noise shrinks, more function evaluations are required for each MCMC step. This behavior is also illustrated in Figure 9, where the CPU time for a single function evaluation is constant, but the time for one MCMC step and for one independent sample increases.

Of course, the number of optimization iterations at each step depends on the choice of stopping tolerance. In these experiments, we fix the function tolerance (see §6.2) to  $10^{-6}$  but normalize the objective function by the standard deviation of the observational noise. This choice imposes an increasingly stringent condition for smaller observational noise, which explains the higher number of function evaluations required. Overall, though, these results suggest that RTO can be applied to inverse problems with extremely small observational noise provided that solving the optimization problems remains tractable.

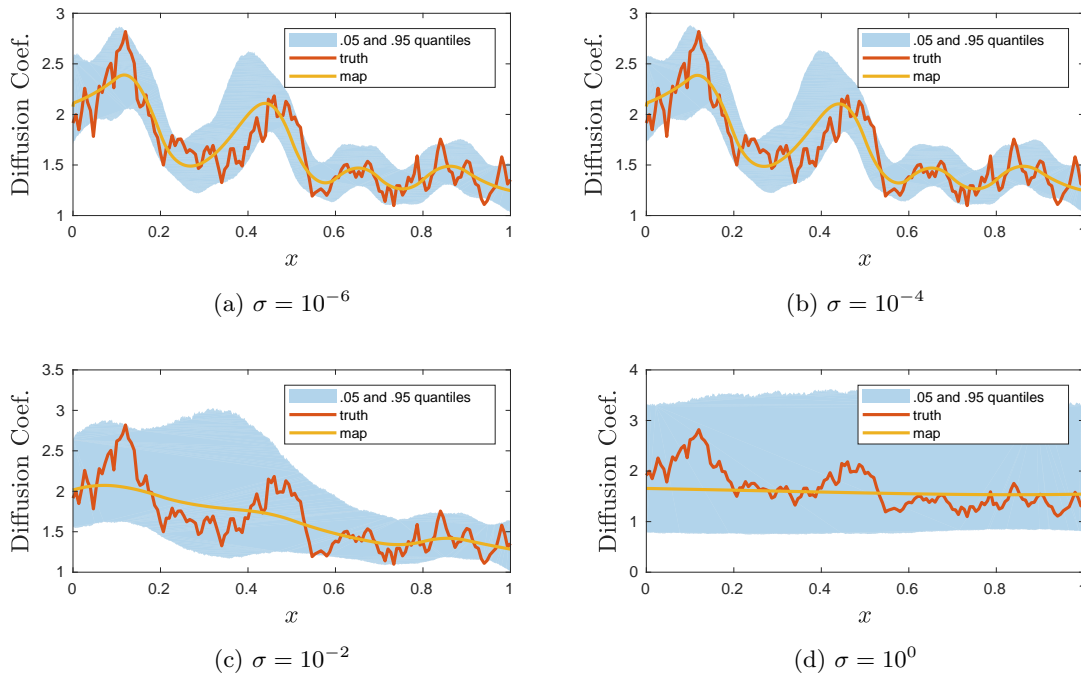


Fig. 8: Posterior distributions computed via RTO-MH with varying observational noise  $\sigma$ . 90% marginal credibility intervals (blue shaded region), true diffusivity coefficient (red line), and MAP estimate (yellow line).

Table 3: Effective sample size (ESS), average acceptance rate, and average number of optimization iterations per step for RTO, for varying observational noise magnitude. Chain length of 5000.

Noise std deviation	$10^{-7}$	$10^{-6}$	$10^{-5}$	$10^{-4}$	$10^{-3}$	$10^{-2}$	$10^{-1}$	$10^0$	$10^1$
Numerical ESS	4504.8	4427.4	4349.9	4423.0	4415.1	4187.2	4317.7	4476.9	5000.0
Acceptance Rate	0.946	0.944	0.941	0.945	0.935	0.924	0.939	0.959	0.999
Opt. Iterations	567.64	495.41	363.71	296.55	89.07	8.32	5.70	4.70	3.31

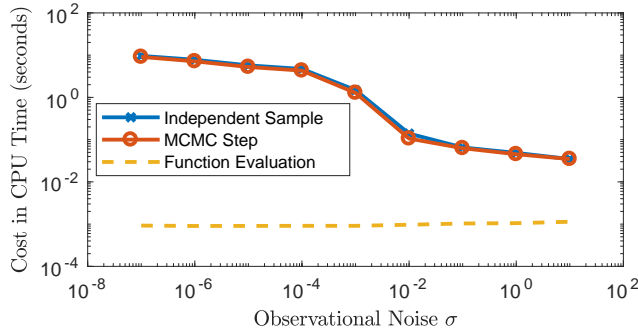


Fig. 9: Computational cost for elements of RTO, varying observational noise.

**6.4. Comparing RTO with pCN.** In our third experiment, we compare the computational efficiency of RTO and pCN [8]. The two algorithms are both dimension-independent. We fix the parameter dimension to  $n = 641$  and compare the algorithms’ performance on inverse problems with different observational noise standard deviations, ranging from  $10^{-6}$  to  $10^0$ . For pCN, we use a chain length of  $5 \cdot 10^6$  and remove the first 50% of the samples as burn-in. We manually tune the step size of pCN to obtain the largest empirical ESS. As shown in Figure 10, the posterior marginals from pCN match those obtained with RTO for the two larger observational noise values. For the two smaller observational noise values, however, pCN does not converge. In particular, examination of Figure 10 and of MCMC trace plots for the smaller noise cases shows that the pCN chain does not travel far from its starting point. Table 4 reveals that RTO requires less computational time per independent sample in *all* cases, even when the observational noise is larger. (Note that this performance metric, time per ESS, normalizes away the impact of different chain lengths.)

In this numerical example, RTO thus outperforms pCN by a large margin. Moreover, in the two cases with smaller observational noise, RTO is the only algorithm that produces meaningful estimates of the posterior. In summary, we find that RTO’s sampling performance is robust to parameter dimension and observational noise, and can be more efficient than pCN.

Table 4: Comparing computational cost for RTO and pCN.

Observational Noise $\sigma$	CPU time (seconds) per ESS	
	RTO	pCN
$10^{-6}$	7.772	$1.193 \cdot 10^{3*}$
$10^{-4}$	4.712	$1.103 \cdot 10^{3*}$
$10^{-2}$	0.139	7.739
$10^0$	0.049	0.250

\*Estimated from a non-converged MCMC chain. Actual values may be higher.

**7. Conclusion.** This paper makes four main contributions. First, we provide two new interpretations for RTO: a geometric viewpoint and a transport map viewpoint that encompasses not only RTO, but other optimization-based samplers. The transport viewpoint provides a foundation for our subsequent results. Second, we introduce a method that substantially improves RTO’s scaling with parameter dimension; this implementation overcomes a primary bottleneck of the original RTO approach. It splits the parameter field into two subspaces and allows us to sample and evaluate densities by solving smaller problems of size  $r$ , where  $r$  is the rank of an SVD that can be

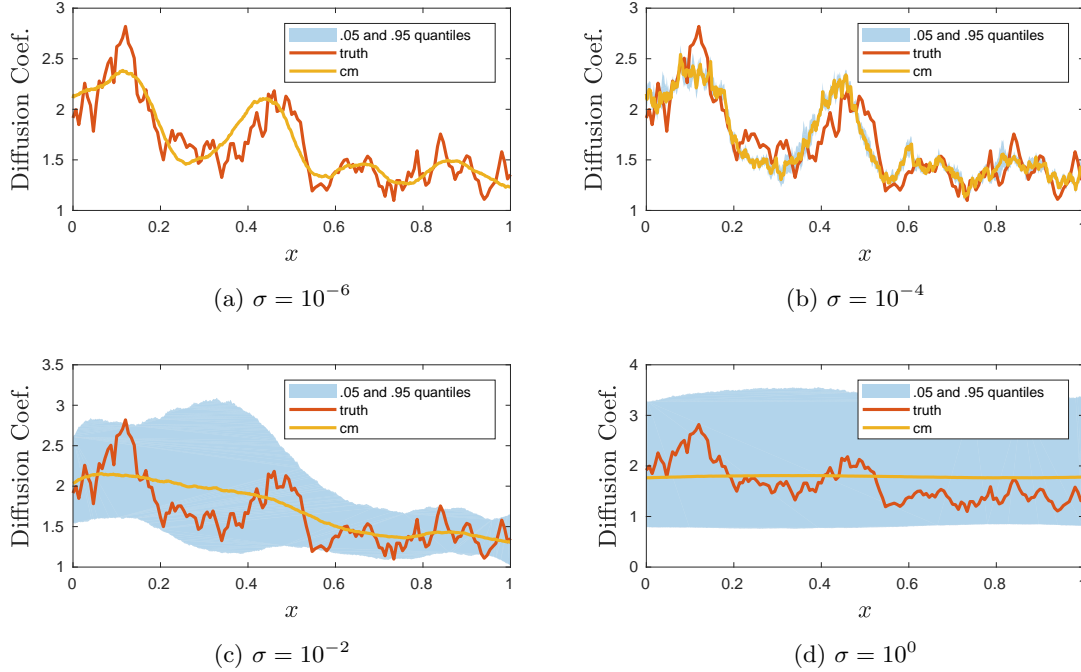


Fig. 10: Posterior distributions computed through pCN, varying observational noise  $\sigma$ . 90% credibility intervals (blue shaded region), true diffusivity coefficient (red line) and CM estimate (yellow line). The MCMC chain does not converge for  $\sigma = 10^{-6}$  and  $\sigma = 10^{-4}$ .

truncated and is bounded by the number of observations. This implementation takes advantage of certain low-dimensional structure in Bayesian inverse problems [10, ?] and makes inference in thousands of parameter dimensions tractable. Third, we develop a theoretical argument for RTO's dimension-independent sampling behavior. The argument involves formulating RTO as a mapping from prior samples to proposal samples in a function space (i.e., infinite-dimensional) setting. We show that the induced proposal measure is absolutely continuous with respect to the prior. With a few additional assumptions, this result implies that the RTO-MH chain is invariant for the posterior distribution. Finally, we provide an empirical exploration of factors influencing the sampling efficiency of RTO. Our numerical results confirm that RTO is dimension-independent, and also show that the observational noise magnitude affects the cost of solving each optimization problem but not the mixing of an RTO Metropolis independence sampler. Despite the increased cost-per-sample of RTO, we find that it outperforms pCN for wide range of problem settings. These results show that it is possible for RTO to tackle inverse problems with high-dimensional parameters and even very small observational noise.

There are many ways to extend the work described here. For example, one might use a mixture of several RTO proposals, defined by different linearizations, to better capture the nonlinearity in some extremely challenging inverse problems. Such mixtures might also help surmount the invertibility issues that arise when the assumptions of Theorem 5 are violated. For instance, one could employ a defensive mixture involving the prior distribution, along with localized proposals that are managed with trust-region strategies. The transport-map interpretation of RTO also suggests combining the RTO map with more sophisticated MCMC proposals on the Gaussian reference space, along the lines of [21]. In addition, since RTO's prior-to-proposal mapping has a well-defined continuum limit, one



can naturally use RTO to generate coupled proposal samples at different discretization levels. These correlated samples can be used as control variates in the multi-level/multi-fidelity setting [13, 11, 22] to further accelerate the computation of posterior statistics.

**Acknowledgments.** We thank Benjamin Zhang for his thoughtful comments and suggestions. J. Bardsley acknowledges support from the Gordon Preston Fellowship offered by the School of Mathematical Sciences at Monash University. T. Cui acknowledges support from the Australian Research Council, under grant number CE140100049 (ACEMS). Y. Marzouk and Z. Wang acknowledge support from the United States Department of Energy, Office of Advanced Scientific Computing Research, AEOLUS Mathematical Multifaceted Integrated Capability Center.

**Appendix A. Implicit sampling and Metropolized RML.** Here we briefly review the transport maps defined by the random-map implementation of implicit sampling [19] and by Metropolized RML [20].

Implicit sampling requires that the target density have level sets that are “star-shaped,” in that any ray starting from the mode passes through each level set exactly once. The target density is written as

$$\exp(-\Phi(v)),$$

where the negative log-target density  $\Phi$  has a minimum at the mode  $v_{\text{MAP}}$ . In order to draw proposal samples, we sample  $\xi \in \mathbb{R}^n$  from a standard Gaussian and solve the following nonlinear system of equations for  $v \in \mathbb{R}^n$ :

$$\begin{cases} \frac{L^{-1}(v - v_{\text{MAP}})}{\|L^{-1}(v - v_{\text{MAP}})\|} = \frac{\xi}{\|\xi\|} \\ \Phi(v) - \Phi(v_{\text{MAP}}) = \frac{1}{2}\|\xi\|^2 \end{cases}.$$

The *direction* of the sample  $v$  (relative to the mode) is based on the direction of the sampled  $\xi$ . The *magnitude* of  $v$  is then found through a one-dimensional line search for the point where the negative log target  $\Phi$  satisfies

$$\Phi(v) - \Phi(v_{\text{MAP}}) = \frac{1}{2}\|\xi\|^2.$$

In practice,  $L$  is chosen to be a square root of the inverse of the Hessian of  $\Phi$  evaluated at the mode.

$$L^\top L := [\nabla^2 \Phi(v_{\text{MAP}})]^{-1}.$$

Metropolized RML requires that the target distribution have a Gaussian prior and additive Gaussian observational noise. For simplicity, we present a whitened version of Metropolized RML where the prior and observational noise covariances are transformed to the identity and the data is shifted to the origin. As in Section 2.1, we assume that the parameter dimension is  $n$  and that the data dimension is  $m$ . Suppose that the target density on the parameter  $v_x \in \mathbb{R}^n$  is then proportional to:

$$\exp\left(-\frac{1}{2}\|v_x\|^2 - \frac{1}{2}\|g(v_x)\|^2\right).$$

Metropolized RML adds the auxiliary variables  $v_d \in \mathbb{R}^m$  and considers an *augmented* target distribution with density proportional to

$$\exp\left(-\frac{1}{2}\|v_x\|^2 - \frac{1}{2}\|g(v_x)\|^2 - \frac{1}{2\gamma(1-\gamma)}\|v_d - g(v_x) + \gamma g(v_x)\|^2\right).$$

This is a distribution on the joint space of parameters and data, but it has the original parameter target distribution as its  $v_x$ -marginal. Now sample  $\xi_x \sim \mathcal{N}(0, I_n)$  and  $\xi_d \sim \mathcal{N}(0, I_m)$  and solve the

following nonlinear system of equations for  $v_x$  and  $v_d$ :

$$\begin{cases} v_x + \frac{1}{\rho} \nabla g(v_x)^\top (g(v_x) - v_d) = \xi_x \\ \frac{1}{\rho} v_d - \left( \frac{1 - \rho}{\rho} \right) g(v_x) = \xi_d \end{cases}.$$

The joint density of the resulting proposal samples in the augmented parameter-and-data space can be calculated. The samples are Metropolized in the augmented space to obtain correlated samples distributed according the augmented target distribution. The components of  $v_x$  are then distributed according to the original target distribution. The parameters  $\rho$  and  $\gamma$  are tunable settings of the algorithm. In practice, they are set close to one and zero respectively.

## REFERENCES

- [1] J. M. BARDSLEY, A. SOLONEN, H. HAARIO, AND M. LAINE, *Randomize-then-optimize: A method for sampling from posterior distributions in nonlinear inverse problems*, SIAM Journal on Scientific Computing, 36 (2014), pp. A1895–A1910, doi:10.1137/140964023.
- [2] A. BESKOS, M. GIROLAMI, S. LAN, P. E. FARRELL, AND A. M. STUART, *Geometric mcmc for infinite-dimensional inverse problems*, Journal of Computational Physics, 335 (2017), pp. 327–351.
- [3] A. BESKOS, G. O. ROBERTS, A. M. STUART, AND J. VOSS, *MCMC methods for diffusion bridges*, Stochastic Dynamics, 8 (2008), pp. 319–350.
- [4] S. BROOKS, A. GELMAN, G. JONES, AND X. L. MENG, eds., *Handbook of Markov Chain Monte Carlo*, Taylor & Francis, 2011.
- [5] B. CALDERHEAD, *A general construction for parallelizing metropolis-hastings algorithms*, Proceedings of the National Academy of Sciences, 111 (2014), pp. 17408–17413.
- [6] A. CHORIN, M. MORZFELD, AND X. TU, *Implicit particle filters for data assimilation*, Communications in Applied Mathematics and Computational Science, 5 (2010), pp. 221–240, doi:10.2140/camcos.2010.5.221.
- [7] P. CONRAD, A. DAVIS, Y. M. MARZOUK, N. PILLAI, AND A. SMITH, *Parallel local approximation mcmc for expensive models*, SIAM/ASA Journal on Uncertainty Quantification, 6 (2018), pp. 339–373.
- [8] S. L. COTTER, G. O. ROBERTS, A. M. STUART, AND D. WHITE, *MCMC methods for functions: modifying old algorithms to make them faster*, Statistical Science, 28 (2013), pp. 424–446, doi:10.1214/13-STS421.
- [9] T. CUI, K. J. H. LAW, AND Y. M. MARZOUK, *Dimension-independent likelihood-informed MCMC*, Journal of Computational Physics, 304 (2016), pp. 109–137, doi:10.1016/j.jcp.2015.10.008.
- [10] T. CUI, J. MARTIN, Y. M. MARZOUK, A. SOLONEN, AND A. SPANTINI, *Likelihood-informed dimension reduction for nonlinear inverse problems*, Inverse Problems, 29 (2014), p. 114015, doi:10.1088/0266-5611/30/11/114015.
- [11] M. B. GILES, *Multilevel monte carlo path simulation*, Operations Research, 56 (2008), doi:10.1287/opre.1070.0496.
- [12] M. GIROLAMI AND B. CALDERHEAD, *Riemann manifold Langevin and Hamiltonian Monte Carlo methods*, Journal of the Royal Statistical Society: Series B (Statistical Methodology), 73 (2011), pp. 123–214, doi:10.1111/j.1467-9868.2010.00765.x.
- [13] S. HEINRICH, *Multilevel monte carlo methods*, Large-Scale Scientific Computing, (2001), pp. 58–67, doi:10.1007/3-540-45346-6.
- [14] D. HIGDON, H. LEE, AND C. HOLLOMAN, *Markov chain monte carlo-based approaches for inference in computationally intensive inverse problems*, in Bayesian Statistics 7, J. M. Bernardo, M. J. Bayarri, J. O. Berger, A. P. Dawid, D. Heckerman, A. F. M. Smith, and M. West, eds., Oxford University Press, 2003, pp. 181–197.
- [15] J. KAIPIO AND E. SOMERSALO, *Statistical and Computational Inverse Problems*, vol. 160 of Applied Mathematical Sciences, Springer Science & Business Media, 2006, doi:10.1007/b138659.
- [16] Y. M. MARZOUK, T. MOSELHY, M. PARNO, AND A. SPANTINI, *Sampling via measure transport: An introduction*, in Handbook of Uncertainty Quantification, R. Ghanem, D. Higdon, and H. Owhadi, eds., Springer, 2016, pp. 1–41, doi:10.1007/978-3-319-11259-6.
- [17] J. C. MATTINGLY, N. S. PILLAI, AND A. M. STUART, *Diffusion limits of the random walk Metropolis algorithm in high dimensions*, The Annals of Applied Probability, 22 (2012), pp. 881–930.
- [18] K. L. MENGESSEN AND R. L. TWEEDIE, *Rates of convergence of the Hastings and Metropolis algorithms*, The Annals of Statistics, 24 (1996), pp. 101–121.
- [19] M. MORZFELD, X. TU, E. ATKINS, AND A. J. CHORIN, *A random map implementation of implicit filters*, Journal of Computational Physics, 231 (2012), pp. 2049–2066, doi:10.1016/j.jcp.2011.11.022.
- [20] D. S. OLIVER, *Metropolized Randomized Maximum Likelihood for sampling from multimodal distributions*, SIAM/ASA Journal on Uncertainty Quantification, 5 (2017), pp. 259–277, doi:10.1137/15M1033320.
- [21] M. PARNO AND Y. M. MARZOUK, *Transport map accelerated Markov chain Monte Carlo*, SIAM/ASA Journal on Uncertainty Quantification, 6 (2018), pp. 645–682, doi:10.1137/17M1134640.

- [22] B. PEHERSTORFER, K. WILLCOX, AND M. GUNZBURGER, *Optimal model management for multifidelity Monte Carlo estimation*, 38 (2016), pp. A3163–A3194, doi:10.1137/15M1046472.
- [23] G. D. PRATO, *An Introduction to Infinite-Dimensional Analysis*, Springer-Verlag Berlin Heidelberg, 2006, doi:10.1007/3-540-29021-4.
- [24] G. O. ROBERTS, A. GELMAN, AND W. R. GILKS, *Weak convergence and optimal scaling of random walk Metropolis algorithms*, The Annals of Applied Probability, 7 (1997), pp. 110–120.
- [25] G. O. ROBERTS AND R. L. TWEEDIE, *Exponential convergence of Langevin distributions and their discrete approximations*, Bernoulli, (1996), pp. 341–363, doi:10.2307/3318418.
- [26] D. RUDOLF AND B. SPRUNGK, *On a generalization of the preconditioned cranknicolson metropolis algorithm*, Foundations of Computational Mathematics, 18 (2018), pp. 309–343.
- [27] A. M. STUART, *Inverse problems: a Bayesian perspective*, Acta Numerica, 19 (2010), pp. 451–559, doi:10.1017/S0962492910000061.
- [28] K. WANG, T. BUI-THANH, AND O. GHATTAS, *A randomized maximum a posteriori method for posterior sampling of high dimensional nonlinear Bayesian inverse problems*, SIAM Journal on Scientific Computing, 40 (2018), pp. A142–A171.
- [29] Z. WANG, J. M. BARDSLEY, A. SOLONEN, T. CUI, AND Y. M. MARZOUK, *Bayesian inverse problems with  $L1$  priors: a Randomize-then-Optimize approach*, SIAM Journal on Scientific Computing, 39 (2017), pp. S140–S166, doi:10.1137/16M1080938.